DOI: 10.1002/ejic.200600797

Synthesis, Structural and Spectroscopic Studies on the Lanthanoid *p*-Aminobenzoates and Derived Optically Functional Polyurethane Composites

Timothy Fiedler,[a][‡] Matthias Hilder,[b] Peter C. Junk,*[b] Ulrich H. Kynast,[a] Marina M. Lezhnina,*[a][‡‡] and Marek Warzala[a]

Keywords: Luminescence / Lanthanoids / Polyurethane composites / Carboxylates

Aromatic carboxylates of the rare earths are known for highly efficient luminescence, thus holding the promise of applicability in optical devices, but may be problematic to apply as such due to their structure, which is polymeric in nature. Therefore, means of conversion into molecular species or eventually polymer embeddings are sought, while at the same time maintaining their advantageous optical features. For these purposes, co-ligations of rare earth *p*-aminobenzoates with bidentate bipyridine and phenanthroline, tridentate terpyridine and polyurethanes, which may also be perceived as polydentate ligands, have been carried out. The materials were characterised with focus on their structure and optical performance. Brightly luminescing composites were obtained from reactions with aromatic and aliphatic diisocyanates. Prolonged UV-irradiation of the materials proved hexamethylene diisocyanates to be superior with regard to photodegradation. Transparent polyurethane monoliths with emission quantum yields between 40 % and 55 % were eventually prepared from covalent attachement of Tb(*p*-aminobenzoate)$_3$ and its bipyridine co-ligated complexes to a hexamethylene diisocyanate/polyol system.

1. Introduction

Efficiently luminescing complexes of the rare earths are not only spectacular visually, but also of interest in numerous photophysical applications, ranging from sensors over light emitting devices (LEDs, OLEDs) to luminescent immunoassays. Practically, it is frequently desirable to incorporate them into matrices in order to render them applicable, or even appropriately functional in corresponding devices. As such, sol-gel matrices, zeolites and various polymers have been utilised.

Although the principle "local" intramolecular luminescence mechanism of the complexes is understood comparably well, especially in β-diketonates,[1–5] a reliable and comprehensive description of the structural factors influencing the optical performance appears to be lacking, especially with regard to carboxylates.

[a] University of Applied Sciences Muenster, Dep. of Chemical Engineering/Applied Materials Sciences,
Stegerwaldstr. 39, 48565 Steinfurt, Germany
Fax: +49-2551-962-187
E-mail: marina@fh-muenster.de
[b] School of Chemistry, Box 23, Monash University,
Clayton, Vic. 3800, Australia
Fax: +61-03-9905-4597
E-mail: peter.junk@sci.monash.edu.au
[‡] Current address: OSRAM GmbH, Phosphor Development & Applications,
Hellabrunner Straße 1, 81543 München
[‡‡]On leave from: Mari Technical State University Yoshkar-Ola, Institute of Physics,
Lenin-pl. 3, 424000 Yoshkar-Ola, Russia

This lack of understanding is particularly true for the group of aromatic carboxylates imbedded in mentioned hosting matrices, which includes some of the most efficiently luminescing rare earth species. Rare earth aromatic carboxylates generally form coordination-polymeric associates with corresponding short-range interactions rather than isolated molecular entities.[6] Resulting insolubility and low vapour pressure pose a practical shortcoming with regard to matrix incorporation schemes, as the destruction of the original rare earth coordination polymer often quenches or diminishes the luminescence efficiencies. Bipyridines ("bipy") and phenanthrolines ("phen"), acting both as co-chelating and co-sensitizing ligands, can help to circumvent the solubility or volatility problem by forming new molecular coordination complexes. At the same time, they can help to keep the immediate chemical environment of the ion free from water, which is frequently encountered in the pure carboxylates. In addition to these bidentate co-ligands, we have additionally used terpyridine ("terpy") as a co-ligand. Also, some matrices may analogously be understood in terms of co-ligation, in that they may also occupy the rare earth coordination sphere in polydentate fashion as well, e.g. oxygen atoms of silica based matrices or silicones.

In this report, we focus on *p*-aminobenzoic acid ("pabaH"), because we learnt from single crystal structure data that the amino group might be chemically accessible for covalent attachment to a matrix on one hand, and, e.g. Tb(*p*-aminobenzoate)$_3$ ["Tb(paba)$_3$"], show intense luminescence

as the pure coordination polymer on the other hand, which can be enhanced by co-coordination,[7] and even be maintained on incorporation into zeolite matrix.[8] While this research was in progress, some of the crystal structures were confirmed by reports from other groups, or were previously published.[9] We will additionally provide results on the interaction of $Tb(paba)_3$, $Tb(paba)_3$phen and $Tb(paba)_3$bipy with isocyanates and eventually a polyurethane matrix and their behaviour under prolonged UV irradiation.

$$LnCl_3{\cdot}n(H_2O) + 3\ Na(paba) \xrightarrow{H_2O} [Ln(paba)_3H_2O]_n + 3\ NaCl \quad (1)$$

$$TbCl_3{\cdot}n(H_2O) + 3\ Na(paba) \xrightarrow[1,10\text{-phen}]{H_2O} [Tb(paba)_3(H_2O)_2]_2{\cdot}2\ H_2O + 3\ NaCl \quad (2)$$

2. Results and Discussion

2.1. Coordination Polymers

A $[Ln(paba)_3{\cdot}H_2O]_n$ series with the members [Ln = Eu (**1**), Gd (**2**) and Tb (**3**); pabaH = *p*-aminobenzoic acid], were conveniently synthesised in good yield by treatment of an aqueous solution of the respective lanthanoid chloride with sodium *p*-aminobenzoate [Equation (1)]. We could also obtain a modified phase of the terbium complex, being the dimeric $[Tb(paba)_3(H_2O)_2]_2{\cdot}2H_2O$ (**4**), which was obtained in a similar manner [Equation (2)], but in the presence of 1,10-phenanthroline, in an attempt to prepare phenanthroline co-coordinated complexes of the series. In the case of compound **4**, phenanthroline was not incorporated in the final product, rather a different structural phase (of a previously published structure[9d]) of the terbium *p*-aminobenzoate was isolated. This was therefore not characterised further because it was a previously known compound.

The FTIR spectra of all compounds showed significant changes in the carbonyl stretching frequency compared with the free ligand (see the representative representation of $[Eu(paba)_3H_2O]$, and $[Tb(paba)_3H_2O]$ in comparison with H(paba) in Figure 1). In *p*-aminobenzoic acid, the C=O stretch occurs at 1655 cm^{-1}, whereas in the lanthanoid complexes, the band is shifted to significantly lower wave numbers and is split into two distinct bands around 1390 and 1500 cm^{-1}. In the compounds **1**–**3** there are increased absorbances in the 3300–3450 cm^{-1} region attributable to water in the metal complexes. The complexes **1**–**3** were pure by Na_2EDTA titration for lanthanoid content and carbon microanalysis for the composition $[Ln(paba)_3H_2O]$ as suggested by the X-ray crystal structures (below).

To ascertain the thermal stability of a representative sample of the $[Ln(paba)_3H_2O]$ series, the Eu analogue was analysed by thermogravimetric analysis. The exothermic release of water (peak maximum at 200 °C), which takes place in the temperature range of 120–220 °C is accompanied by a weight loss of 3% which is identical to the weight loss expected for the stated composition. This reaction can be described by Equation (3).

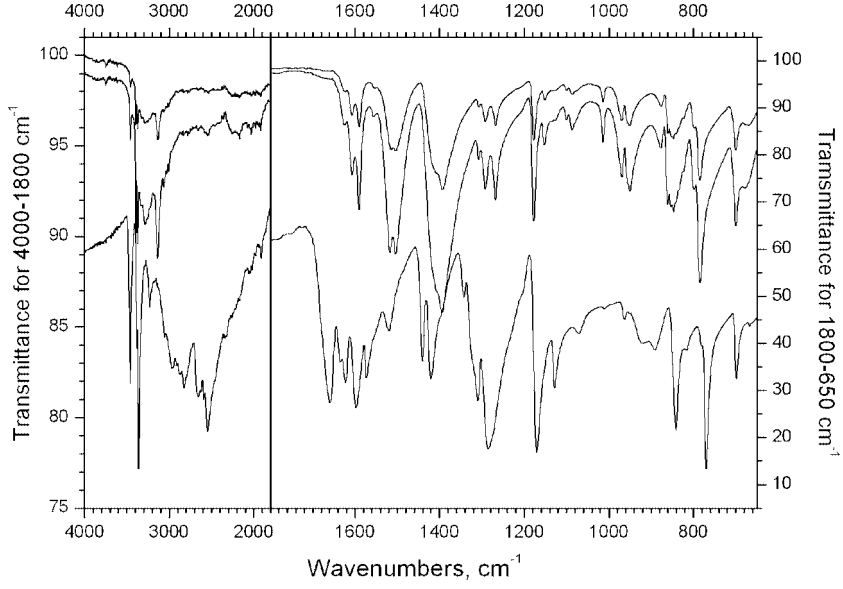

Figure 1. FTIR spectra of H(paba) (bottom), $Tb(paba)_3H_2O$ (middle) and $Eu(paba)_3H_2O$ (top).

$$Eu(C_6H_4NH_2COO)_3(H_2O) \rightarrow Eu(C_6H_4NH_2COO)_3 + H_2O \quad (3)$$

The thermal decay starts at 330 °C and continues to 810 °C. It is accompanied by several endothermic events (390, 430, 500, and 740 °C). Although the slope of the TG curve is very steady, there is a slight change in the gradient (330–460 °C) accompanied by a weight loss of 30%. This is the weight loss expected for the formation of the dimeric europium benzoate complex connected by an oxo bridge. A plausible reaction sequence is shown in Equations (4), (5) and (6).

$$Eu(C_6H_4NH_2COO)_3 + 3\ O_2 \rightarrow Eu(C_6H_5COO)_3 + 1.5\ H_2O + 3\ NO \quad (4)$$

$$Eu(C_6H_5COO)_3 + 7.5\ O_2 \rightarrow Eu(C_6H_5COO)_2(OH) + 2\ H_2O + 7\ CO_2 \quad (5)$$

$$2\ Eu(C_6H_5COO)_2(OH) \rightarrow (C_6H_5COO)_2Eu{-}O{-}Eu(C_6H_5COO)_2 + H_2O \quad (6)$$

In the range of 460–810 °C the final oxidation product is formed. The total mass loss of 70% is very close to the expected (69%) as shown in Equation (7).

$$(C_6H_5COO)_2Eu{-}O{-}Eu(C_6H_5COO)_2 + 30.5\ O_2 \rightarrow Eu_2O_3 + 10\ H_2O + 28\ CO_2 \quad (7)$$

Single crystals of compound **2** were grown by slow concentration of aqueous samples and its solid-state structures determined using X-ray crystallography. $[Gd(paba)_3H_2O]_n$ is isomorphous and structurally identical to that previously published for $[Ln(paba)_3H_2O]_n$ Ln = La, Ce, Pr, Nd, Sm, Eu, Tb, Dy, Er,[9] effectively establishing this structural type for the lighter and larger lanthanoids extends to Ln = Er. Compound **2** crystallises in the monoclinic space group $P2_1/n$ with one whole monomeric unit in the asymmetric unit. The lanthanoid metal centre is eight coordinate being bound by one chelating carboxylate, four monodentate carboxylates, one water molecule and perhaps surprisingly, one $N_{(amino)}$ group [Figure 2, a)]. Each of the monodentate carboxylate groups bridge to an adjacent Ln centre, while the chelating carboxylate is solely bound to one Ln centre. The overall structure is thus a three-dimensional polymeric species [Figure 2, b)] which is additionally extended through O–H···O and N–H···O hydrogen bonds. The Ln–O and Ln–N bond lengths (see Figure 2, caption) demonstrates well the lanthanoid contraction when compared with the other lanthanoid analogues,[9] with all internuclear distances about the Ln centres diminishing across the series in line with the reduction in ionic radii of the metal.[10] It is rather surprising that the lanthanoid centre is coordinated by an amine, given the compound was crystallised from water. It may be expected that water would complete the coordination sphere of the oxophilic rare-earth metal and presumably, binding of the amine to the metal, arises from a packing effect. It is worthy to mention the Ln···Ln internuclear distances, particularly with respect to the possibility of Ln···Ln energy transfer (see later). The Ln···Ln distances for this series of compounds are approximately 4.50 to 4.80 Å and for compound **2**, this distance is 4.725(3) Å.

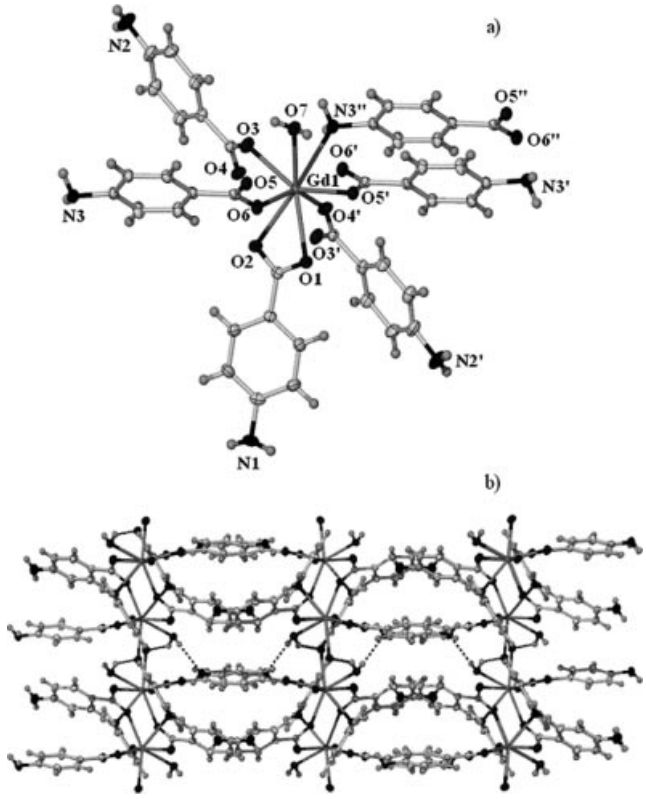

Figure 2. a) X-ray crystal structure of coordination sphere about Gd in polymeric $[Gd(paba)_3]\cdot H_2O$ (**2**). Thermal ellipsoids are at the 50% probability level. Selected bond lengths [Å]: Gd(1)–O(1) 2.461(2), Gd(1)–O(2) 2.455(2), Gd(1)–O(3) 2.336(2), Gd(1)–O(4) 2.304(2), Gd(1)–O(5) 2.342(2), Gd(1)–O(6) 2.349(3), Gd(1)–O(7) 2.513(3), Gd(1)–N(3) 2.668(3). b) X-ray crystal structure of polymeric $[Gd(paba)_3]\cdot H_2O$ (**2**). Thermal ellipsoids are at the 50% probability level.

Single crystals of compound **6** suitable for X-ray diffraction studies were grown from an aqueous solution of $[Tb(paba)_3H_2O]_n$ in the presence of 1,10-phenanthroline. The structure of this phase of the terbium analogue is isomorphous to that established for $[Ln(paba)_3(H_2O)_2]_2\cdot 2H_2O$ (Ln = Tb,[9d] Dy,[11] Ho,[9d] Y,[9d] Yb,[9d,12] Lu[9d]) and thus an example of the heavier structural type for the *p*-aminobenzoates of the lanthanoids and will not be discussed further. Significantly, by crystallisation of the terbium analogue as both structural phases, the structural boundary for the lanthanoid *p*-aminobenzoates existing as a dimer has now been established to start at Tb ranging to Lu, while the polymeric phase extends from La to Er. The reason for the isolation of two different phases presumably lies in the mode of crystallisation. We isolated the dimer phase in the presence of 1,10-phenanthroline and this presumably affects the solubility of the polymeric phase.

X-ray powder diffraction patterns of bulk material of compounds **1** to **3** were compared with patterns calculated from X-ray single crystal experiments and established that the structure of the bulk materials in all cases was identical to that obtained in the single crystals.

The Tb^{3+} analogue of this series showed significant and exploitable luminescence in the visible, while Eu^{3+} is quenched by charge-transfer states and MLCT,[13] additionally supported by vibrational quenching.[14] Gd^{3+} is known to promote ligand phosphorescence at 24445 cm^{-1},[15] we observe corresponding broad emission bands in $Gd(paba)_3$ at 420 nm and 478 nm, however, accompanied by a comparably strong emission due to minute Tb^{3+} impurities (see below).

The luminescence of $Tb(paba)_3$ relies on the following successive steps:[16,17] 1. singlet–singlet absorption of the ligand ($^1S_0 \rightarrow {}^1S^*$, π–π in nature), 2. intersystem crossing (ISC, $^1S^* \rightarrow {}^3T$, promoted by the spin-orbit coupling due to the Tb^{3+} ion), 3. (exchange resonance driven) energy transfer Ligand(^3T)$\rightarrow Tb^{3+}(^5D_4)$. Emission, excitation end reflectance spectra of solid $Tb(paba)_3H_2O$ are given in Figure 3.

As may be seen clearly, excitation can most efficiently be accomplished in this complex at a comparably short wavelength of approximately 310 nm. The quantum yield of the complex amounts to an unexpectedly high value (88%, e.g. λ_{exc} = 340 nm), which is very surprising in view of the coordination of both, -NH_2 and OH_2 as ligands, as they are usually both essential vibrational deactivators of the excited state. However, it should be noted that both the Ln–OH_2 distance (261 pm) and the Ln–NH_2 distance (276 pm) are fairly long and multiphoton emission may thus be of secondary importance only, which is even more pronounced due to fairly strong hydrogen bonding.

A significant shortcoming for further utilisation of the complexes is that their strong degree of association [see Figure 2, b)] prevents, for example, evaporation without decomposition or dissolution in aprotic organic solvents. We could obtain solutions from $[Tb(paba)_3H_2O]$ only in refluxing DMF, albeit to a high cost in luminescence efficiency.

2.2. Co-coordinated Complexes

To explore further the luminescence properties of derivatives of the paba series above, we co-coordinated $[Tb(paba)_3H_2O]$ with the bidentate ligands bipyridine and phenanthroline as well as the tridentate terpyridine. The complexes were accessed by crystallisation from solutions of pabaH and bipy, phen, or terpy, respectively, in ethanol, to which aqueous $TbCl_3$ was added. In order to identify the immediate Tb^{3+} coordination environment in the complexes obtained {$[Tb(paba)_3(bipy)(H_2O)]_2 \cdot 2H_2O$ (**5**), $[Tb(paba)_3(phen)(H_2O)]_2 \cdot 2H_2O$ (**6**), $[Tb(paba)_3(terpy)(H_2O)]_2 \cdot 6.7H_2O$ (**7**)}, single crystals grown from these solutions by slow evaporation were subjected to single-crystal structure analyses. The X-ray crystal structure of $[Tb(paba)_3(bipy)(H_2O)]_2 \cdot 2H_2O$ was previously reported.[18] For comparison, the La and Eu and analogues involving 1,10-phenanthroline were also structurally investigated. It is of importance to understand the structural variation of the rare earth series when investigating their luminescence properties. For example, we have shown that in the coordination polymer $Na[Tb(pic)_4] \cdot 1.5H_2O$ (picH = 2-picolinic acid) one-dimensional energy migration occurs, which can be utilised to transfer energy to Eu^{3+} if the latter is co-doped into the material.[19] However, co-doping is only successful in these compounds, if the structural integrity of the parent compound is not compromised, a factor, which we have observed in the above-mentioned picolinates, if lanthanum was introduced. Therefore, we typically address the structural characteristics of several of the lanthanoid series.

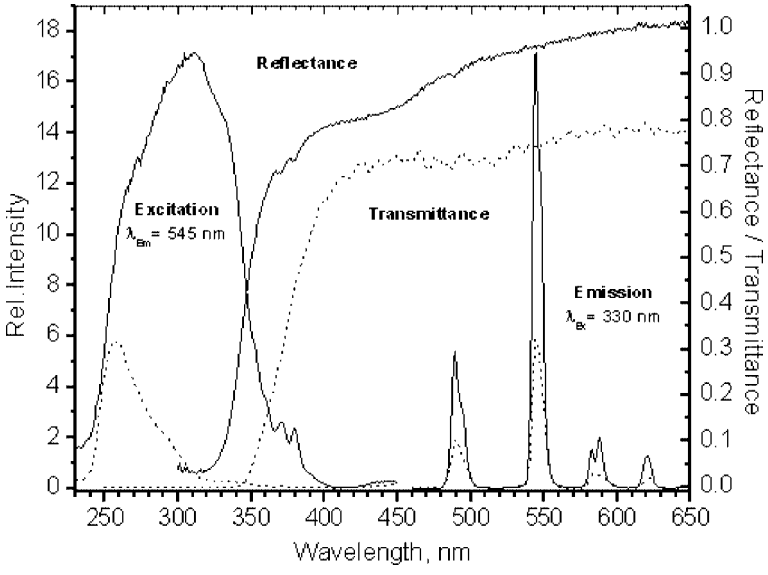

Figure 3. Comparison of optical spectra of the free complex $Tb(paba)_3H_2O$ (powder, solid line) and the polymer composite $Tb(paba)_3$PU (monolith, broken line).

Therefore, we also present the X-ray structural characterisation of $[Eu(paba)_3(phen)(H_2O)]_2{\cdot}2H_2O$ (**8**) and $[La(paba)_3(pabaH)(phen)_2]{\cdot}H_2O$ (**9**). Additional support for the significance of detailed structural data will be provided at the end of this paragraph.

In the published structure of $[Tb(paba)_3(bipy)(H_2O)]_2{\cdot}2H_2O$ (**5**) the compound exists as a dimer, with each terbium atom eight-coordinate. Each Tb atom is bound by a bidentate bipy ligand, a monodentate water molecule and three carboxylates, each with different binding modes. One carboxylate is chelating bidentate, the second is a monodentate-bound ligand, while the third bridges to the other Tb atom. There is a water molecule in the lattice and the *p*-amino groups of the paba ligands are not coordinated to the Tb atoms. The Tb···Tb distance in the dimer is 5.554(3) Å, thus allowing energy migration between the ions within the dimer.

$[Tb(paba)_3(phen)(H_2O)]_2{\cdot}2H_2O$ (**6**) crystallises in the triclinic space group $P\bar{1}$ with one whole monomer comprising the asymmetric unit. The compound dimerises through hydrogen bonding from a Tb-bound water molecule to the O atom of a Tb-bound carboxylate group (Figure 4). Each Tb atom is nine-coordinate, being bound by a bidentate 1,10-phenanthroline ligand, three chelating bidentate carboxylate groups and a water molecule. There are also two lattice water molecules per hydrogen-bonded dimer. The Tb···Tb distance in the hydrogen-bonded dimer is 5.884(5) Å. $[Eu(paba)_3(phen)(H_2O)]_2{\cdot}2H_2O$ (**8**) is isomorphous with **6** (Figure 4).

Figure 4. X-ray crystal structure of dimeric, hydrogen-bonded $[Tb(paba)_3(phen)(H_2O)]_2{\cdot}2H_2O$ (**6**); hydrogen atoms on the aromatic groups are omitted for clarity. Thermal ellipsoids are at the 50% probability level. $[Eu(paba)_3(phen)(H_2O)]_2{\cdot}2H_2O$ (**8**) is isostructural.

In compound **8** the Eu···Eu distance is 5.909(5) Å and is slightly longer due to the larger ionic radius of Eu over Tb.[10]

$[Tb(paba)_3(terpy)(H_2O)]_2{\cdot}6.7H_2O$ (**7**) crystallises in the triclinic space group $P\bar{1}$ with one whole $[Tb(paba)_3(terpy)(H_2O)]_2$ dimer and another half dimer (as well as 10 lattice water molecules) comprising the asymmetric unit. Each Tb atom is nine-coordinate, being bound by a tridentate terpy molecule, a monodentate water molecule, a bidentate carboxylate group, a monodentate carboxylate group and a monodentate carboxylate group that bridges to the other Tb atom (Figure 5). The Tb···Tb distance in this dimer is 5.312(8) Å.

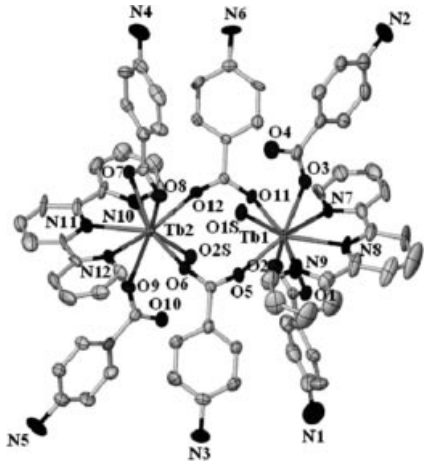

Figure 5. X-ray crystal structure of dimeric, hydrogen-bonded $[Tb(paba)_3(terpy)(H_2O)]_2{\cdot}H_2O$ (**7**); hydrogen atoms on the aromatic groups are omitted for clarity. Thermal ellipsoids are at the 50% probability level.

$[La(paba)_3(pabaH)(phen)_2]{\cdot}H_2O$ (**9**) crystallises in the monoclinic space group $P2_1/c$ with one whole mononuclear unit and one lattice water molecule comprising the asymmetric unit of the structure. The nine-coordinate lanthanum centre is now bound by two bidentate 1,10-phenanthroline ligands, one bidentate carboxylate, two unidentate carboxylate and one unidentate carboxylic acid molecule (Figure 6). It is significant that the lanthanum centre is now bound by a unidentate carboxylic acid molecule rather than by water (or ethanol) molecules, from which the compound was crystallised.

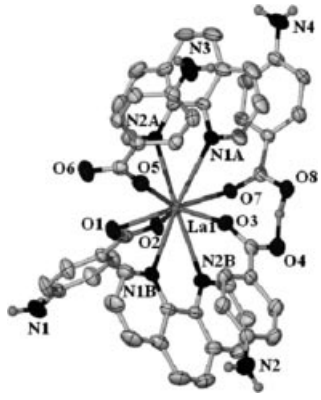

Figure 6. X-ray crystal structure of mononuclear $[La(paba)_3(pabaH)(phen)_2]_2$ (**9**); hydrogen atoms on the aromatic groups are omitted for clarity. Thermal ellipsoids are at the 50% probability level.

The proton on the bound carboxylic acid molecule is involved in hydrogen bonding with one of the O atoms of a unidentate bound carboxylate group. The fact that this compound is a new structural type for this chemistry, and

also that it is mononuclear is exciting, because we now intend to expand this chemistry to the Eu and Tb analogues, where luminescence may be enhanced due to decreased possibility of Ln···Ln quenching. The shortest La···La distance in compound **9** is 10.594(2) Å.

In all compounds comprising the bidentate bipy or phen or tridentate terpy, bond lengths are unexceptional between ligands and metal centres. A noteworthy feature of these compounds, when compared with the parent $[Ln(paba)_3(H_2O)]$ compounds, is that the *para*-nitrogen atoms of the paba group are not involved in binding to the lanthanoid centre (cf. above).

The optical properties of $[Tb(paba)_3(bipy)(H_2O)]_2{\cdot}2H_2O$ and $[Tb(paba)_3(phen)(H_2O)]_2{\cdot}2H_2O$ are depicted in Figure 7. In comparison to $[Tb(paba)_3{\cdot}H_2O]_n$ the excitation maximum has been red-shifted by approximately 50 nm on bipy-co-coordination and about 70 nm on phen-co-coordination $[Tb(paba)_3(bipy)(H_2O)]_2{\cdot}2H_2O$.

This redshift is of high applicatory interest; because the excitation now falls in the range of commercially available and ever improving semiconductor LED excitation sources, and may thus be used in a broader range of low-cost devices. Furthermore, the quantum yield of $[Tb(paba)_3(bipy)(H_2O)]_2{\cdot}2H_2O$ now even amounts to 95% under excitation at 350 nm. This somewhat unusual result may, just as argued for $[Tb(paba)_3H_2O]$ above, once more be interpreted in terms of the molecular structure, displaying long Tb–OH_2 distances and hydrogen bonding. Unfortunately, that high a quantum efficiency is not maintained in $[Tb(paba)_3(phen)(H_2O)]_2{\cdot}2H_2O$, where a drop to 38% is measured at 380 nm.

It was furthermore striking to us to note that the short Ln···Ln distances of 4.725(3) Å found in $[Gd(paba)_3H_2O]$ have an immediate impact on the luminescence spectra: terbium impurities (sub-percent level, $< 0.01\%$) in the Gd complex lead to a strong Tb^{3+} emission, which had approximately 10 times the intensity of the corresponding ligand phosphorescence. Characteristically, the sensitisation of Tb^{3+} is already 4 times weaker in $[Gd(paba)bipy(H_2O)_2]$ (Ln···Ln ca. 5.5 Å) and is not detectable in $[Gd(paba)phen(H_2O)_2](H_2O)_{1.5}$. (Ln···Ln ca. 5.9 Å). This behaviour signals the importance of detailed structural data in the interpretation of luminescent properties. Unfortunately, suitable crystals of the Gd analogue to $[La(paba)_3(pabaH)(phen)_2](H_2O)$ with a La···La distance 10.594(2) Å could not be obtained as yet, but may in the future be an interesting system to evaluate the details of Ln···Ln energy transfer in rare earth metallo-organic complexes.

2.3. Reactions with Isocyanates

The amino group of the paba complexes appeared to be a suitable reaction centre for the attachment of the complexes to polymeric backbones, isocyanates and polyurethanes ("PUs") in particular. As suitable polymer matrices,

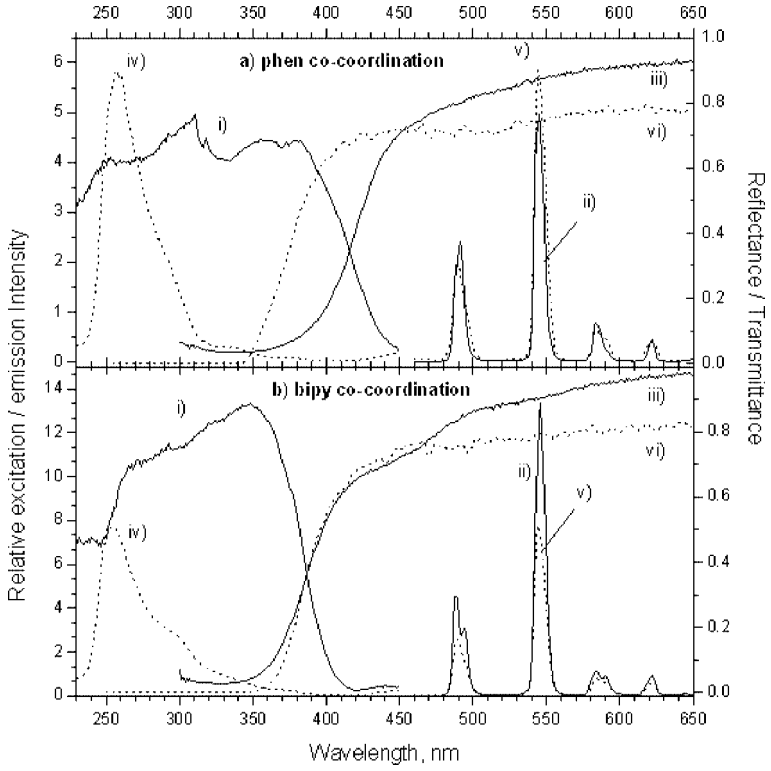

Figure 7. Comparison of free and polymer-imbedded complexes. Top, solid line: $Tb(paba)_3phen$; broken line: $Tb(paba)_3phenPU$. Bottom, solid line: $Tb(paba)_3bipy$; broken line: $Tb(paba)_3bipyPU$. i) excitation, ii) emission ii) reflectance of pure complexes; iv) excitation, v) emission, vi) reflectance of PU composites.

hexamethylene diisocyanates [O=C=N–$(CH_2)_6$–N=C=O, "HDIs"] and derived prepolymers were chosen rather than e.g. methylenebis(1,4-phenylene) diisocyanate (O=C=N–C_6H_4–CH_2–C_6H_4–N=C=O, "DPDIs") or 1,4-phenylene diisocyanate (O=C=N–C_6H_4–N=C=O, "PDIs"), because their optical transparency still allows optical measurements of the complexes imbedded, which might otherwise be obscured due to the extended π electrons, if DPDIs or PDIs were chosen as the matrix. However, reactions of $Tb(paba)_3$ with pure HDI, PDI and MDI were tested as "concentrated polymers" without further crosslinkers [see reaction schemes Figure 8, Equation (8)]. In the following, "$Tb(paba)_3$HDI", "$Tb(paba)_3$PDI" and "$Tb(paba)_3$DPDI" exclusively designate the reaction products of $Tb(paba)_3$ with HDI, PDI and DPDI, respectively, according to Equation (8), while "$Tb(paba)_3$PU" refers to a complete polyurethane matrix, based on HDI and a polyol, in which doping with $Tb(paba)_3$ substitutes a corresponding amount of the polyol [Equation (9)]. Analogously, $Tb(paba)_3$bipy and $Tb(paba)_3$phen have been reacted with HDI and polyol to give $Tb(paba)_3$bipyPU and $Tb(paba)_3$phenPU. The "concentrated" polymeric $Tb(paba)_3$PDI, $Tb(paba)_3$DPDI and $Tb(paba)_3$HDI are obtained as white powders, which are insoluble in all polar and apolar solvents tested; it was not possible to obtain transparent layers or monoliths from these materials. The excitation spectra of these reaction products are represented in Figure 9 in comparison to $Tb(paba)_3$; the corresponding emission spectra only differ in intensities and are not reproduced. Evidently, PDI linkage leads to a slight increase in intensity accompanied by a redshift of the excitation maximum to approximately 330 nm. Unfortunately, due to cloudiness (i.e. light scat-

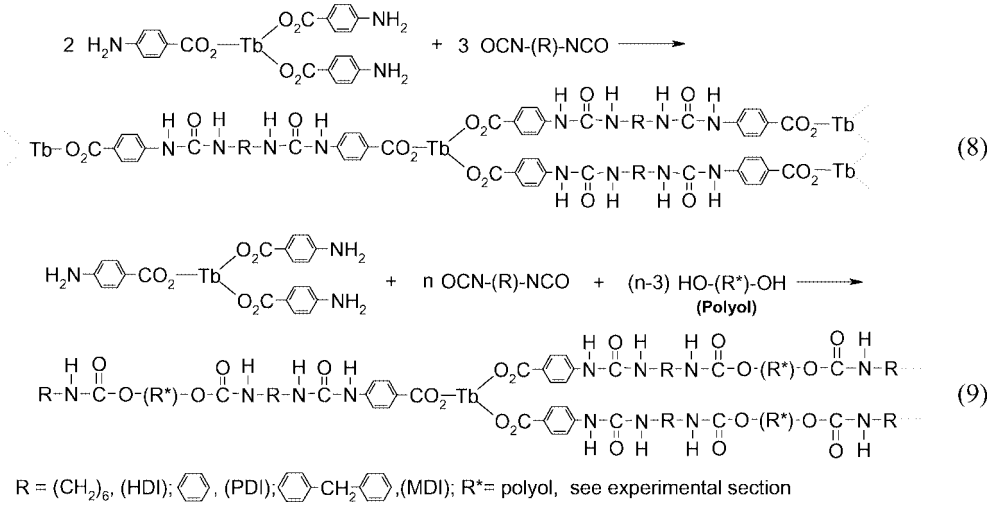

Figure 8. Reaction schemes of $Tb(paba)_3$ and diisocyanates formation of "concentrated" polymeric $Tb(paba)_3$ diisocyanates, Equation (8). Formation of PU-polymer "doped" with $Tb(paba)_3$, Equation (9).

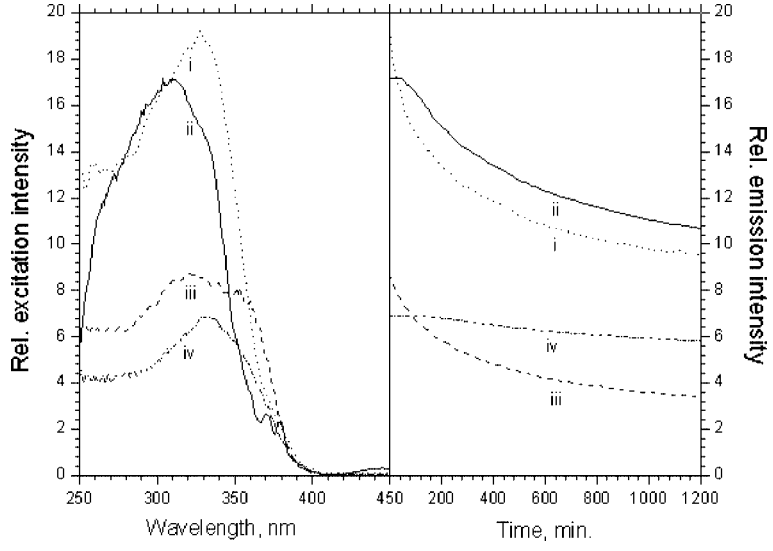

Figure 9. Reaction products of $Tb(paba)_3$ with different diisocyanates. Left: excitation spectra. Right: Photodegradation. i) $Tb(paba)_3$PDI; ii) $Tb(paba)_3$; iii) $Tb(paba)_3$DPDI; iv) $Tb(paba)_3$HDI, see text.

tering), shape and morphology of the polymer layers, reliable data on quantum efficiencies could not be determined, however, a crude visual comparison with diluted samples of $Tb(paba)_3$ in PU [$Tb(paba)_3$PU, see following paragraph] suggests comparable efficiencies.

Transparent composite materials, $Tb(paba)_3$PU, could eventually be prepared using DMF solutions of $Tb(paba)_3$ in a polyol (see experimental section), to which HDI was added [Equation (9)] in Figure 8, R = $(CH_2)_6$. As opposed to that, for reasons not obvious to us, the reactions of polyol-dissolved $Tb(paba)_3$ with PDI and DPDI only gave turbid products. The optical spectra of transparent $Tb(paba)_3$-PU are given in Figure 3. The comparison with pure $Tb(paba)_3$ immediately demonstrates the shortcomings of the composite. The onset of absorption is red-shifted to approximately 400 nm due to matrix contributions, which do not produce a noteworthy emissive response down to 320 nm, while the excitation maximum is blueshifted to 260 nm. The overall emission quantum yield is thus reduced by a factor of two to four (42%, λ_{exc} = 260 nm; 17%, λ_{exc} = 300). However, some error in this value may arise from differing sample and reference shapes (see Exp. Sect.). Correspondingly, the extended conjugation brought about by the –C_6H_4–NH–CO–NH– substituents [see Figure 8, Equation (2)] may be held responsible for the redshift of the absorption. At the same time, the coordination numbers of six for the Tb^{3+} ion, as sketched for simplicity in Figure 8, is most unlikely in the polymer. Instead, coordination of N and O atoms of neighbouring fragments may be expected, thus giving rise to radiationless deactivation by high frequency vibrations.

The initial idea of using bipyridine and phenanthroline as co-ligands to increase their solubility in the (pre-)polymers did not lead to the desired results with respect to efficiency. Although bipyridine co-coordinated $Tb(paba)_3$ could eventually be used to form a clear polymer ["$Tb(paba)_3$bipyPU"], if the $Tb(paba)_3$bipy was initially dissolved in excess HDI followed by addition/crosslinking with polyol, its efficiency is again lowered by a factor of two to three (55%, λ_{exc} = 260 nm to 28%, λ_{exc} = 300 nm) in comparison to pure $Tb(paba)_3$. If $Tb(paba)_3$bipy was dissolved in the polyol prior to HDI addition, bipyridine appeared to be liberated, as indicated by the excitation spectrum, which is then again in resemblance of $Tb(paba)_3$PU, albeit at much lower intensity, at least partly due to the radiation "lost" to bipy absorption. This behaviour is yet more pronounced and evident in $Tb(paba)_3$phen, where a blue emission of phen indicates the presence of the uncoordinated co-ligand. The emission of phen is here seen to a similar extent, regardless of the addition sequence (dissolution in polyol followed by addition of HDI, or dissolution in HDI, followed by polyol admixture). The loss of phen is clearly visible from the spectral agreement of $Tb(paba)_3$PU (broken line in Figure 3) with $Tb(paba)_3$phenPU (broken line in Figure 7, a); the substitution of the bidentate co-ligands by the polydentate polymer fragments may then be interpreted in terms of an entropy increase. Due to the blue ligand emission, we refrained from the determination of quantum yields of $Tb(paba)_3$phenPU, but from the excitation spectra, they may be estimated to amount to > 40% under 260 nm excitation.

For eventual applications of the polymers described, knowledge on further material parameters next to the optical performance will be required, among them the durability and stability of the emission intensity. We have therefore also invested some effort into the characterisation of the emissive properties under prolonged irradiation with UV light. For this purpose, pressed sample polymer disks of approximately uniform thickness of approximately 1 mm to grant complete absorption were irradiated and the depreciation of the Tb^{3+} 545 nm emission line ($^5D_4 \rightarrow {}^7F_5$) was monitored. For comparison, pure $Tb(paba)_3$ was pressed to a powder disk and included in the series. The results of the ageing experiments on $Tb(paba)_3$PDI, $Tb(paba)_3$DPDI and $Tb(paba)_3$HDI and $Tb(paba)_3$ are contained in Figure 9.

The evaluation of the depreciation of $Tb(paba)_3$PDI, which shows the highest initial efficiency, reveals that a maintenance crossover with pure $Tb(paba)_3$ is reached after only a few minutes, indicating that the aromatic polymer backbone of PDI is liable to relatively fast photodegradation. Similarly, $Tb(paba)_3$DPDI shows very similar degradation behaviour, albeit at a lower efficiency level. Remarkably, the aliphatic HDI based polymer is comparably stable, even more so than the pure complex. All curves could be fitted as single exponentials, if the initial degradation delay observed for $Tb(paba)_3$ and $Tb(paba)_3$HDI was taken into account. Based on extrapolation, the maintenance level of $Tb(paba)_3$HDI can accordingly be estimated to amount to almost 80% after 10000 h of operation. Future efforts will thus be directed towards luminescence improvement of aliphatic polyurethanes.

Conclusions

Stimulated by high luminescence efficiencies of *p*-aminobenzoates of Tb^{3+} (quantum yields > 80%), detailed structural investigations have been performed in order to derive materials from $Tb(paba)_3$, which are applicable in photoluminescenct applications, e.g. luminescent markers, or, eventually electrooptical devices, such as OLEDs. Typically, in the series of rare earth *p*-aminobenzoates coordination polymers are formed, which were broken down to molecular species for further manufacture. Such can in part be accomplished using chelating ligands such as bipyridine, phenanthroline, or terpyridine, although crystal structure determinations reveal that they essentially still exist as dimeric units and disadvantageously contain coordinated water. Nevertheless, on co-coordination of with bipyridine, a slight increase in quantum yield is accomplished (> 90%) in the case of Tb^{3+}, while phenanthroline reduces the overall efficiency (36%). The *p*-aminobenzoates of Tb^{3+} were linked to aliphatic and aromatic diisocyanates through the benzoate amino group, yielding brightly green luminescing, insoluble polymer composites. Consecutively, transparent polyurethane monoliths incorporating backbone-linked *p*-

aminobenzoates of Tb^{3+} and co-ligated complexes could be fabricated using aliphatic diisocyanates, and polyols as additional components. These "doped" polyurethanes show photoluminescence with quantum yields in the range between 40 and 55%, albeit at lowered excitation wavelengths. In anticipation of potential applications, the photodegradation of some aromatic and aliphatic composites were evaluated. In these experiments, aliphatic polymer backbones proved to be superior, but had lower initial efficiencies. Future work will thus focus on increasing the *p*-aminobenzoate composite efficiencies. Additionally, we are currently testing other benzoic acid derivatives.

Experimental Section

Lanthanoid salts were purchased from Rhodia, Chempur and Aldrich with specified purity levels of in excess of 99.9%; *p*-aminobenzoic acid was obtained from Aldrich. All starting materials were used without further purification. Deionised water was used in all syntheses. Infrared spectra were recorded on sodium chloride plates as Nujol mulls or pressed into KBr disks (Figure 1) on a Perkin–Elmer Spectrum One FTIR spectrometer. Lanthanoid metal analyses were determined titrimetrically using the Na_2EDTA method. Carbon analyses were carried out using a C-analyser with IR-detection unit (ELTRA, Germany). Melting points were performed in unsealed tubes.

Synthesis: The complexes **1**–**3** were synthesised following a similar procedure. Thus, sodium *p*-aminobenzoate (obtained by the reaction of the free *p*-aminocarboxylic acid with sodium hydrogencarbonate) was added to and aqueous solution of lanthanoid chloride. The crystals were obtained from slightly acidic aqueous medium. The samples were evaporated until large crystals of the complexes deposited. Complex **4** was synthesised in a similar manner, except 1,10-phenanthroline was added to the reaction mixture. Details of the properties for each compound follow. Yields reported are for isolated crystalline material. Yields of these reactions can be enhanced by precipitation of the compounds by addition of acetone to a saturated aqueous solution or increasing the pH value to just below 8 with 2 M ammonia.

$[Eu(paba)_3(H_2O)]$ (1): V_{Eu}: 2.43 cm^3 (0.52 mol/dm^3) = 1.26 mmol. $m_{H-p-ABA}$: 0.52 g = 3.79 mmol. $m_{product}$: 0.68 g (yield 93.0%). $C_{21}H_{20}EuN_3O_7$: calcd. C 43.6, Eu 26.3; found C 43.4; Eu 26.5. FTIR: see Figure 1. Powder XRD: 7.72 (s), 9.96 (s), 15.56 (m), 18.50 (w), 20.04 (m), 22.38 (w), 23.74 (m), 24.16 (m), 24.98 (w), 27.50 (w), 28.54 (w), 29.48 (w), 30.02 (w), 30.96 (w), 32.52 (w), 33.62 (w), 36.78 (m), 37.08 (m), 38.46 (s), 39.68 (w), 40.64 (w), 42.00 (w), 42.92 (w), 44.04 (w), 44.72 (s), 45.76 (w), 46.70 (w), 47.60 (w), 49.42 (w). DTA: 200 °C (exothermic), 390 °C (endothermic), 430 °C (endothermic), 500 °C (endothermic), 740 °C (endothermic). DTG: 120–220 °C (3% weight loss), 330–460 °C (30%), 460–810 °C (69% weight loss).

$[Gd(paba)_3(H_2O)]$ (2): Yield 17%. IR (Nujol): $\tilde{\nu}$ = 3400 m (br), 1660 s, 1595 s, 1567 s, 1399 m, 1347 s, 1306 w, 1297 m, 1260 w, 1240 w, 1163 m, 1149 w, 1093 w, 1051 w, 1013 w, 848 w, 787 m, 760 m, 698 s, 634 m cm^{-1}. $C_{21}H_{20}GdN_3O_7$: calcd. C 43.00; found C 43.08.

$[Tb(paba)_3(H_2O)]$ (3): V_{Tb}: 2.30 cm^3 (0.58 mol/dm^3) = 1.34 mmol. $m_{H-p-ABA}$: 0.55 g = 4.01 mmol

$m_{product}$: 0.72 g (yield 92.0%). $C_{21}H_{20}N_3O_7Tb$: calcd. C 43.1, Tb 27.3; found C 43.9, Tb 27.2.. FTIR: see Figure 1. Powder XRD: 7.72 (s), 10.00 (s), 14.88 (m), 15.56 (m), 18.38 (w), 18.76 (w), 19.46 (w), 20.04 (m), 21.62 (w), 22.34 (m), 23.74 (m), 24.12 (m), 24.92 (m), 27.44 (w), 28.54 (w), 28.98 (w), 29.52 (w), 30.04 (w), 30.42 (w), 31.06 (w), 32.80 (w), 33.74 (w), 35.48 (w), 36.62 (m), 37.22 (w), 38.56 (w), 39.80 (w), 40.58 (w), 42.10 (m), 44.00 (w), 44.72 (m), 45.70 (w), 47.82 (w).

$[Tb(paba)_3(H_2O)_2]_2{\cdot}2H_2O$ (4): From one attempted synthesis of co-crystallising $[Tb(paba)_3(H_2O)]$ with phenanthroline, we obtained crystals of the title compound that were isostructural with the previously reported complex.[9d] Unit cell data for compound **4**: triclinic, space group $P\bar{1}$ (No. 2), a = 10.7819(7), b = 12.0981(8), c = 13.2695(9) Å, α = 72.407(1), β = 66.679(1), γ = 87.981(1)°, V = 1508.0(2) $Å^3$.

$[Tb(paba)_3(bipy)(H_2O)]_2{\cdot}2H_2O$ (5) and $[Tb(paba)_3(phen)(H_2O)]_2{\cdot}2H_2O$ (6), $[Tb(paba)_3(terpy)(H_2O)]_2{\cdot}6.7H_2O$ (7), $[Eu(paba)_3(phen)(H_2O)]_2{\cdot}2H_2O$ (8) and $[La(paba)_3(pabaH)(phen)_2].H_2O$ (9), $[Gd(paba)_3(bipy)(H_2O)]_2{\cdot}2H_2O$ (10) $[Gd(paba)_3(phen)(H_2O)]_2{\cdot}2H_2O$ (11): $[Tb(paba)_3(bipy)(H_2O)]_2{\cdot}2H_2O$ was prepared by adding an aqueous solution of $TbCl_3$ (0.25 g) to an ethanol/water (C_2H_5OH/H_2O, 1:1) solution of *p*-aminobenzoic acid (0.2 g) and bipyridine (0.3 g), to give a volume of ca. 30 mL. The colourless crystals were obtained by slowly evaporating the mixture at room temperature for several days.

Analogously, the preparation of $[Ln(paba)_3(phen)(H_2O)]_2{\cdot}2H_2O$, [Ln = Eu, (**8**) Tb (**6**), Gd (**11**)] involved the addition of an aqueous $LnCl_3$ (Eu, Tb, Gd) solution (0.2 g) to an ethanol solution of *p*-aminobenzoic acid (0.3 g) and 1,10 phenanthroline (0.3 g) after two weeks in an open vessel afforded small light yellow crystals suitable for single crystal structure determination.

"Working amounts" of **5**, **6**, **10** and **11** were obtained using H(paba) (3 mmol) and bipy (or phen) (2 mmol), dissolved in of water/ethanol mixture (20 mL, 1: 1), adjustment of the pH to 5 using 2 M ammonia solution. An aqueous solution of Tb^{3+} [1 mmol of from of 0.5 M $TbCl_3$ ($GdCl_3$) stock solution] was then slowly added to the ligand solution under vigorous stirring. Almost complete and immediate precipitation occurs after slowly raising the pH of this solution to just below 8.0. The complexes were filtered and dried at 60 °C. The products deviated in their composition from the material used for crystal structure determination due to the drying procedure (loss of lattice water): $[Gd(paba)_3bipy(H_2O)_2]$: calcd. C 48.95; found 48.96; $[Gd(paba)_3phen(H_2O)_2](H_2O)_{1.5}$: calcd. C 48.83; found C 48.90].

For the synthesis of crystals of $[Tb(paba)_3(terpy)(H_2O)]_2{\cdot}6.7H_2O$ (**7**) terpyridine (0.3 g) and *p*-aminobenzoic acid (0.2 g) were dissolved in 50% ethanol (3 mL). To the resulting clear solution, $TbCl_3$ solution (0.2 g in 3 mL water) was added dropwise. The reaction was stirred for 5 h. A few light-yellow crystals were received on partial evaporation of the solvent.

Single crystals of $[La(paba)_3(pabaH)(phen)_2]{\cdot}H_2O$ (**9**) were prepared as for compounds **6** and **8** except $LaCl_3$ solution was used in place of $LnCl_3$(Ln = Eu, Tb).

$Tb(paba)_3HDI$, $Tb(paba)_3PDI$ and $Tb(paba)_3DPDI$: The complex polymer composites were synthesised by adjusting a procedure described in the literature.[20] All operations were carried out providing for the exclusion of water (standard Schlenk techniques). Vacuum dried $Tb(paba)_3$ (10^{-3} mbar, 140 °C, 5 h, 0.010 mol) was dissolved in dry DMF (20 mL). To this solution the pure diisocyanate (0.017 mol) was added dropwise. The reaction was carried out within 14 h at 80 °C under argon. After solvent evaporation, the residue was dried in vacuo and powdered using a mortar and pestle.

$Tb(paba)_3PU$, $Tb(paba)_3bipyPU$ and $Tb(paba)_3phenPU$: For the preparation of the transparent polyurethanes a commercial system consisting of a hexamethylene diisocyanate prepolymer and a polyol was used (from Lackwerke Peters, 47906 Kempen, Germany, VT 3402 KK). To determine the exact amounts of polyol to be substituted by the corresponding Tb complexes, the NCO content was determined using chlorobenzene as solvent, dibutylamine as reagent and bromothymol blue as the indicator for the HDI, for the OH number of the polyol, pyridine, phthalic anhydride and phenolphthalein were used, according to procedures previously described.[21] Analytically, 5.40 mmol NCO/g diisocyanate and 5.34 mmol OH/g polyol were found.

To obtain dilute samples for efficiency measurements, the complexes (2 mmol) were dissolved in DMF and added to the hexamethylene diisocyanate (1 g, ratio paba: NCO group approximately 1:100), DMF was evaporated in vacuo and the complex solution in diisocyanate thus obtained was mixed with the polyol (1:1 ratio), the mixture was placed in a transparent cuvette of 1 cm path length, air bubbles were removed under vacuum. The polymerisation to give the polyurethane was carried out at 60 °C in a drying chamber. Polymers containing more than $1{\cdot}10^{-2}$ mol complex/L could be prepared in an analogous manner. For such samples, the consumption of HDI by $Tb(paba)_3$ or was accounted for in that a lower amount of polyol was used. However, the emission intensities (not quantum yields) were at a maximum at approximately $1{\cdot}10^{-2}$ mol complex/L.

Optical Characterisation: All emission and excitation intensities in the spectra reproduced are scaled against each other, such as to grant direct comparability.

Emission and excitation spectra of the solids were recorded at an angle of incidence of ca. 50° using a praying mantis type of set up to allow horizontal sample positioning without a cover. Reflectance spectra were obtained using an integrating sphere with a diameter of 70 mm and 10 mm port openings vs. commercial white and black references (Labsphere), and $BaSO_4$, respectively. Two Acton 300 Monochromators of 300 mm focal length were thus synchronously scanned. The intensity of the 450 W Xe source was detected with an Acton Photomultiplier tube P2, the gratings had 1200 gmm^{-1}. The excitation spectra of $Tb(paba)_3HDI$, $Tb(paba)_3PDI$ and $Tb(paba)_3DPDI$ presented in Figure 9 were corrected for the lamp and spectrometer profiles with $BaMgAl_{10}O_{17}$: Eu ("BAM"). $Tb(paba)_3$, $Tb(paba)_3bipy$, $Tb(paba)_3phen$ were also measured against Lumogen Red doped PMMA powders (doping level 50 ppm), whose quantum yield was taken as a constant 42% in the excitation range between 250 nm and 500 nm. Relative quantum yields of the clear PU composite monoliths [$Tb(paba)_3PU$, $Tb(paba)_3bipyPU$, $Tb(paba)_3phenPU$], prepared in 1 cm cuvettes, were determined relative to a Lumen Red/PMMA disk of 3 mm thickness. Due to the confinement in the reference disk of lower thickness, some loss due to lateral propagation of emitted light within the disk is possible, but could not be accounted for, because neither sample cuvette nor reference disk could be inserted into the integrating sphere. Additionally, we would like to point out that the quantum efficiencies given, while reproducible within our optical setup, may still carry imprecisions, not the least owing to the lack of a suitable green emitting standard with continuous quantum yield in the spectral excitation range between 250 and 500 nm (estimated imprecision margin ±10%). However, the general trends described and discussed will not be affected.

The photochemical degradation data of the samples presented in Figure 9 were collected under irradiation with a 150-W Xe lamp that was shone onto an area of 400 cm^2 through a UV band pass filter (from Schott, Germany, UG11, 3 mm). The change of emission was monitored through a green interference filter (from LOT-Oriel, 64293 Darmstadt, Germany, 546FS10-50) and focussed on a CCD camera (from Acton Research, Spectrum MM) through a Nikon® lens at a distance of 25 cm. Light source, filters and detection unit were attached to a housing, which contained the samples at the bottom. A freshly prepared Al mirror (thermal evaporation, 25 cm^2) was used to turn the horizontally entering beam onto the samples at the bottom, the camera was aligned on top of the housing. Background radiation was accounted for by subtraction of $BaSO_4$ measurements prior to interpretation.

Xray Crystallography Studies: For all compounds X-ray quality crystals were sealed and mounted in thin-walled capillaries, with hemispheres of data collected at room temperature with a Bruker SMART CCD diffractometer (Mo-K_α radiation, λ = 0.71073 Å) using the omega scan mode. Data sets were corrected for absorption using the program SADABS.[22] For all structures, the position of the heavy atoms were found using the Patterson method for heavy atoms and refined on F^2 using SHELXL97–2[23] with X-SEED as the graphic interface.[24] All non-hydrogen atoms were located and were refined with anisotropic thermal parameters. Hydrogen atoms were placed in calculated positions (riding model) and were not refined. For compounds **2**, **6**, **8** and **9** hydrogen atoms were located on the NH_2 groups and on water molecules and were refined isotropically. For compound **7** hydrogen atoms were not located on heteroatoms and were not included in the refinement. Crystal data, and a summary of data collection are listed below.

CCDC-607965 (for **2**), -607966 (for **6**), -607967 (for **7**), -607968 (for **8**) and -607969 (for **9**) contain the supplementary crystallographic data for this paper. These data can be obtained free of charge from The Cambridge Crystallographic Data Centre via www.ccdc.cam.ac.uk/data_request/cif.

Crystal Data for Compound 2: $C_{21}H_{20}GdN_3O_7$, M = 583.65, $0.24\times0.18\times0.15$ mm, monoclinic, space group $P2_1/n$ (No. 14), a = 9.7452(9), b = 22.736(2), c = 9.8229(9) Å, β = 99.9290(10)°, V = 2143.9(3) $Å^3$, Z = 4, D_c = 1.808 g/cm^3, $F(000)$ = 1148, 9744 reflections collected, 3072 unique (R_{int} = 0.0665). Final $GooF$ = 1.045, R_1 = 0.0287, wR_2 = 0.0691, R indices based on 2639 reflections with $I>2\sigma(I)$ (refinement on F^2), 323 parameters, 0 restraints. Lp and absorption corrections applied, μ = 3.142 mm^{-1}.

Crystal Data for Compound 6: $C_{33}H_{30}N_5O_8Tb$, M = 783.54, $0.36\times0.35\times0.32$ mm, triclinic, space group $P\bar{1}$ (No. 2), a = 10.4554(8), b = 12.3129(9), c = 14.0035(10) Å, α = 92.8650(10), β = 102.8890(10), γ = 109.0390(10)°, V = 1646.4(2) $Å^3$, Z = 2, D_c = 1.581 g/cm^3, $F(000)$ = 784, 7545 reflections collected, 4665 unique (R_{int} = 0.0461). Final $GooF$ = 1.050, R_1 = 0.0466, wR_2 = 0.1283, R indices based on 4260 reflections with $I>2\sigma(I)$ (refinement on F^2), 466 parameters, 15 restraints. Lp and absorption corrections applied, μ = 2.206 mm^{-1}.

Crystal Data for Compound 7: $C_{230}H_{228}N_{38}O_{66}Tb_6$, M = 5534.02, $0.32\times0.30\times0.15$ mm, triclinic, space group $P\bar{1}$ (No. 2), a = 17.460(3), b = 18.615(3), c = 19.377(3) Å, α = 80.199(3), β = 72.342(3), γ = 73.823(3)°, V = 5738.3(14) $Å^3$, Z = 1, D_c = 1.601 g/cm^3, $F(000)$ = 2792, 26873 reflections collected, 16542 unique (R_{int} = 0.0803). Final $GooF$ = 1.011, R_1 = 0.0768, wR_2 = 0.1882, R indices based on 9943 reflections with $I>2\sigma(I)$ (refinement on F^2), 1531 parameters, 0 restraints. Lp and absorption corrections applied, μ = 1.918 mm^{-1}.

Crystal Data for Compound 8: $C_{33}H_{30}EuN_5O_8$, M = 776.58, $0.20\times0.20\times0.20$ mm, triclinic, space group $P\bar{1}$ (No. 2), a = 10.4543(11), b = 12.2021(13), c = 14.0607(15) Å, α = 92.904(2), β

= 102.593(2), γ = 108.734(2)°, V = 1643.6(3) Å^3, Z = 2, D_c = 1.569 g/cm^3, F(000) = 780, 7553 reflections collected, 4692 unique (R_{int} = 0.0394). Final *GooF* = 1.071, R_1 = 0.0537, wR_2 = 0.1398, R indices based on 4315 reflections with $I > 2\sigma(I)$ (refinement on F^2), 465 parameters, 15 restraints. Lp and absorption corrections applied, μ = 1.966 mm^{-1}.

Crystal Data for Compound 9: $C_{52}H_{43}LaN_8O_9$, M = 1062.85, 0.40 × 0.40 × 0.20 mm, monoclinic, space group $P2_1/c$ (No. 14), a = 18.8602(12), b = 19.7204(13), c = 13.1888(9) Å, β = 97.1610(10)°, V = 4867.1(6) Å^3, Z = 4, D_c = 1.450 g/cm^3, F(000) = 2160, 22150 reflections collected, 6988 unique (R_{int} = 0.0646). Final *GooF* = 1.003, R_1 = 0.0340, wR_2 = 0.0648, R indices based on 5324 reflections with $I > 2\sigma(I)$ (refinement on F^2), 676 parameters, 0 restraints. Lp and absorption corrections applied, μ = 0.943 mm^{-1}.

Acknowledgments

We acknowledge the Australian Research Council for continued support. We also acknowledge an IPRS scholarship and Monash Graduate Scholarship (to M.H.) and funding by the Bundesministerium für Bildung und Forschung (BMB+F Grant 17 094 00) to M.W. BAM and Lumogen Red references were generously provided by Philips Research Laboratories (Aachen, Germany) and BASF (Ludwigshafen, Germany), respectively.

[1] S. Sato, S. M. Wada, *Bull. Chem. Soc. Jpn.* **1970**, *43*, 1955.
[2] W. R. Dawson, J. L. Kropp, M. Windsor, *J. Chem. Phys.* **1966**, *45*, 2410.
[3] O. L. Malta, *J. Lumin.* **1997**, *71*, 229.
[4] F. R. G. e Silva, O. L. Malta, *J. Alloys Compd.* **1997**, *250*, 427.
[5] G. F. G. F. de Sá, O. L. Malta, L. de Mello Donegá, A. R. Simas, R. L. Longo, P. A. da Silva Jr., E. F. Santa Cruz, *Coord. Chem. Rev.* **2000**, *196*, 165.
[6] A. Ouchi, Y. Suzuki, Y. Ohki, Y. Koizumi, *Coord. Chem. Rev.* **1998**, *92*, 29.
[7] B. Yan, H. Zhang, *Mater. Res. Bull.* **1998**, *10*, 1517.
[8] D. Sendor, P. C. Junk, U. Kynast, *Solid State Phenomena* **2003**, *90/91*, 521.
[9] a) M. S. Khiyalov, I. R. Amiraslanov, Kh. S. Mamedov, E. M. Movsumov, *Zh. Strukt. Khim. (J. Struct. Chem.)* **1981**, *22*, 113; b) S.-Y. Niu, Y.-L. Zhang, W. Lai, Z.-Z. Yang, G.-D. Yang, L. Ye, *Huaxue Xuebao* **2001**, *59*, 2170; c) S. Y. Niu, G. D. Yang, Y. L. Zhang, J. Jin, L. Ye, Z. Z. Yang, *J. Mol. Struct.* **2002**, *608*, 95; d) H.-L. Sun, C.-H. Ye, X.-Y. Wang, J.-R. Li, S. Gao, K.-B. Yu, *J. Mol. Struct.* **2004**, *702*, 77; e) C.-H. Ye, H.-L. Sun, X.-Y. Wang, J.-R. Li, D.-B. Nie, W.-F. Fu, S. Gao, *J. Solid State Chem.* **2004**, *177*, 3735.
[10] R. D. Shannon, *Acta Crystallogr., Sect. A* **1976**, *32*, 751.
[11] Z. Rzaczynska, V. K. Belskii, *Pol. J. Chem.* **1994**, *68*, 309.
[12] L. Z. Rzaczynska, V. K. Belskii, *Pol. J. Chem.* **1994**, *68*, 309.
[13] S. T. Frey, W. D. Horrocks Jr., *Inorg. Chem.* **1991**, *30*, 1073.
[14] G. Blasse, B. C. Grabmeier, *Luminescent Materials*, Springer, **1994**.
[15] B. Yan, S. B. Wang, J. Z. Ni, *Monatsh. Chem.* **1998**, *129*, 151.
[16] V. L. Ermolaev, V. G. Aleshin, E. A. Saenko, *Dokl. Akad. Nauk* **1965**, *165*, 1048.
[17] M. W. S. Sato, *Bull. Chem. Soc. Jpn.* **1970**, *43*, 1955.
[18] L. Oyang, H.-L. Sun, X.-Y. Wang, J.-R. Li, D.-B. Nie, W.-F. Fu, S. Gao, K.-B. Yu, *J. Mol. Struct.* **2005**, *740*, 175.
[19] D. Sendor, M. Hilder, T. Juestel, P. C. Junk, U. H. Kynast, *New J. Chem.* **2003**, *27*, 1070.
[20] C.-L. Lin, H.-M. Mao, R.-R. Wu, P.-L. Kuo, *Macromolecules* **2002**, *35*, 3083.
[21] Z. Wirpsza, *Poliuretany, Chemia technologia zastosowanie*, WNT Warszawa, **1991**.
[22] R. H. Blessing, *Acta Crystallogr., Sect. A* **1995**, *51*, 33.
[23] G. M. Sheldrick, *University of Göttingen*, **1997**.
[24] L. J. Barbour, *J. Supramol. Chem.* **2001**, *1*, 189.

Received: August 29, 2006
Published Online: November 13, 2006

